Hindawi
Wireless Communications and Mobile Computing
Volume 2019, Article ID 5287679, 8 pages
https://doi.org/10.1155/2019/5287679

Research Article

A Compact Ku-Band Active Electronically Steerable Antenna with Low-Cost 3D T/R Module

Zheng Xu,[1] Chengxiang Hao,[1] Kuiwen Xu,[2] and Shichang Chen [2]

[1] *The University of Chinese Academy of Sciences, Beijing 101400, China*
[2] *The Key Lab of RF Circuits and Systems of the Ministry of Education of China, Hangzhou Dianzi University, Hangzhou 310018, China*

Correspondence should be addressed to Shichang Chen; eechensc@hdu.edu.cn

Received 9 November 2018; Revised 21 March 2019; Accepted 14 April 2019; Published 22 April 2019

Guest Editor: Sungchang Lee

This paper presents a novel compact Ku-band active electronically steerable antenna array design with a low-cost and integrated T/R 3D module employed for airborne synthetic aperture radar (SAR) systems. The entire system adopts 3D multilayer technology with vertical interconnection to construct the hermetically packaging RF modules. By assembling different multifunctional modules into a whole multilayer board, the 3D T/R technique greatly improves the system integration and reduces implementation cost and size. Besides, a wideband circular polarized antenna array was designed in LTCC and connected to the proposed T/R modules to form a complete AESA. The whole proposed antenna system has been fabricated and experimentally investigated. Measurement results showed very good phased array performances in terms of gain, axial ratio, and radiating patterns. The low-cost, lightweight, and low-power features exhibited by the proposed design validate its applicability for weight and power constrained platforms with great electronic steering ability.

1. Introduction

Radar imaging is widely used in applications such as geographical mapping [1], security surveillance [2], and collision avoidance [3]. Among many diversified solutions, the synthetic aperture radar (SAR) is a very powerful one because it can synthesize a large aperture to yield increased resolution by using coherent processing of multiple observations from a moving antenna [4].

On the other hand, due to the quick advancements of airborne techniques represented by the unmanned aerial vehicle (UAV) recently, SAR systems start to appear in some airborne platforms. This significantly extends the mobility, flexibility, and economic efficiency of this special radar. It is well known that the successful implementation of a SAR demands a high performance active electronically steerable antenna (AESA), which is a vital and widespread technique that is commonly utilized in various military and civil applications, such as weather monitoring [5], aircraft surveillance [6], space satellite communication [7], and imagining [8]. To meet the stringent requirements of power and loading capacity for an airborne system, the AESA must be designed as compact and lightweight. As the most important components in an AESA, the transmit/receive module (TRM) and radiating antenna array are therefore demanded to be power efficient, broadband, dimensionally small, and widely steerable.

To reduce the footprint of TRM, a preliminary 3D packaging concept that vertically stacks multiple submodules has been proposed in the literature [9–11]. Some well-established processes represented by the low temperature cofired ceramics (LTCC), which are particularly suitable for the manufacture of RF modules, are often applied to assemble several MMICs or discrete chips and that can be fabricated with low cost [12, 13]. Passive components can be placed at various layers, and 3D integration enables the compactness of modules. Besides, owing to the high dielectric constant and the low dielectric and conductor losses, the LTCC technology is also widely used in the design of millimeter-wave antenna arrays [14–16]. Moreover, given the advantages of small size, low profile, and light weight, the patch antennas with LTCC technique are getting more attention for phased array implementations [16, 17].

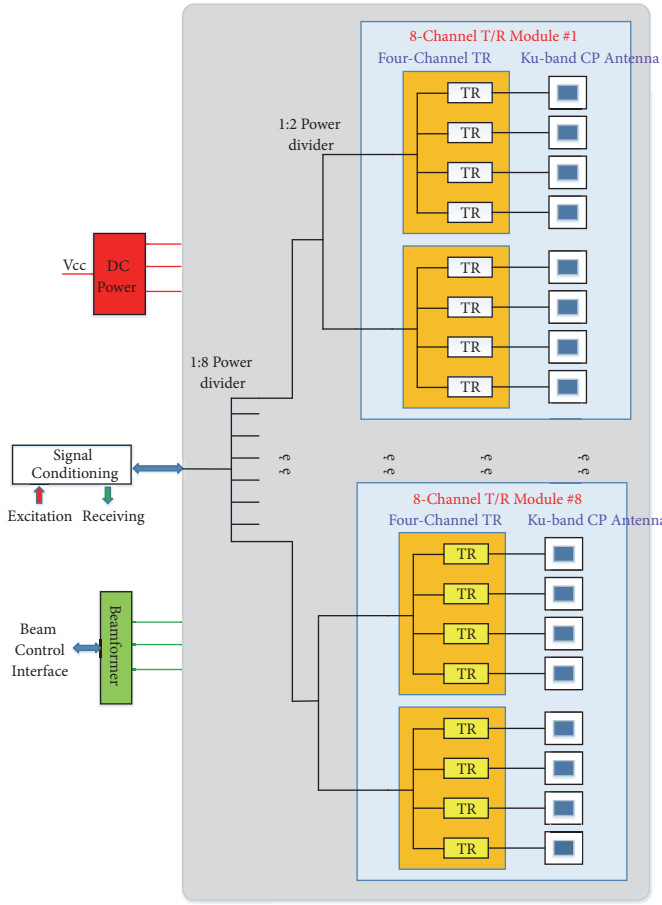

Figure 1: Schematic diagram of the proposed active electronically steerable antenna (AESA) system.

In this work, a Ku-band AESA with low cost and compact T/R 3D module for airborne SAR systems is devised with a reduced overall implementation cost and rapid prototyping speed. The remainder of this paper is organized as follows: the whole system is briefly introduced in Section 2. The design details of the TRM and antenna array are given in Section 3. Section 4 shows the simulation and measurement results of the devised system. Section 5 finally gives the conclusion.

2. System Overview

2.1. AESA Architecture. The main motivation of this work is to design a compact and cost-effective AESA system intended for airborne synthetic aperture radar in Ku-band. The main electrical and mechanical specifications are listed as follows:

(1) operation frequency: 15~16 GHz

(2) array size: 8 × 8

(3) beam width: 12°

(4) scan range: ±60° @azimuth direction, ±60°@range direction

(5) polarization: right-handed circular

(6) axial ratio: ⩽3 dB

(7) beam switching time: ⩽20 uS

(8) beam steering error: ⩽0.5°

(9) EIRP: ⩾24.4 dBW

(10) size: 100 × 100 × 50 mm3

(11) maximum power: ⩽100 W

(12) antenna weight: ⩽1 Kg.

Figure 1 shows the schematic diagram of the proposed AESA system. According to the listed requirements above, the AESA is designed at the center frequency of 15.5 GHz, with a 1 GHz bandwidth. It is mainly comprised of eight active sub-modules; each module constitutes an eight-channel 3D T/R module which drives a Ku-band circular polarized antenna array. The antenna features a rectangular grid alignment; the distance between each radiating element is 9.5 mm (roughly $\lambda_g/4$), in both azimuth and range directions.

The architecture of the whole system can be divided into three distinct layers. The top one is the radiating layer, where a compact and low-profile microwave antenna array is designed. The middle layer is intended for T/R modules and heat dissipation. The T/R module is aligned in the azimuth direction, containing eight channels. The entire AESA has eight parallel T/R modules in the range direction. This middle layer is connected to the radiating layer through the RF

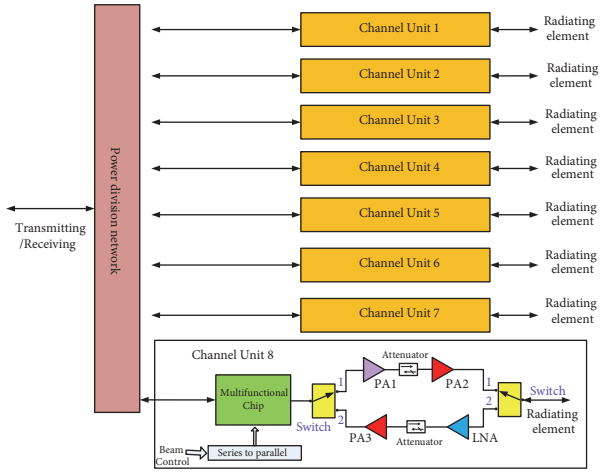

FIGURE 2: Diagram of the proposed AESA system.

SSMP connectors, with the help of structural fixture. The bottom layer is reserved for a multifunctional board which contains feeding network, beam control, power distribution, and so on. It connects to the middle layer through the RF SSMP and low-frequency connectors, providing beam control instructions, DC power, and RF signal.

3. Module Design

3.1. Low-Cost 3D T/R Module. As it is well known, the T/R module is one of the most crucial modules in a front end. It produces a high-power signal that drives antenna in the transmitting mode and amplifies weak signal got from antenna for further processing in the receiving mode. The selection of T/R module solution should comprehensively consider factors like electrical characteristics, hardware reliability, maintainability, and cost. Besides, the channel number, interface type, and structure should also be optimized in order to achieve the best overall array performances.

Figure 2 shows the diagram of the devised T/R module. In this particular work, the proposed T/R module integrates eight channels. A one-to-eight power divider is included; every output terminal drives an independent T/R unit (depicted in the zoomed-in insert), which is further connected to a radiating antenna array. Each single unit physically contains a receiving path, a transmitting path, and a common path. To achieve large system integrity and guarantee reliability, the transmitting and receiving paths share a common multifunctional chip which integrates a 6-bit phase shifter and frequency synthesizer. The link budget (signal level budget) of the front end is carefully calculated in the Keysight SystemVue software [18]. Transmission line and relevant interconnect losses are considered together with the gain characteristics of chips. Deliberate tradeoffs are made to ensure a best system performance. Meanwhile, adequate design tolerances are reserved to prevent possible failure due to component variation.

As the low-noise amplifier (LNA) and power amplifier (PA) elements have different RF performance specifications, discrete chips are used and connected with the multifunctional chip.

As known to all, the noise figure and gain of first stage largely affect the overall noise performance of the receiving channel. As the receiving channel requires very high gain, a two-stage configuration is adopted for the LNA design. A GaAs LNA chip with 1.5 dB noise figure is used for the first stage. Because the total loss of interconnect, switch, and bonding wire is about 1 dB, the overall noise figure is therefore 2.5 dB. Regarding the transmitting channel, the combination of a GaAs PA and driver chip is applied. Herein, to have good amplitude and phase balance, a 6-bit digitally controlled attenuator is added to the T/R module along with the high resolution phase shifter in the multifunctional chip. Figure 3 depicts the basis specification distribution diagram of the proposed AESA.

In order to reduce system implementation cost and save circuit size and weight as well as prototyping time, a cost-effective multilayer PCB technique is used. To be specific, a microwave board and an analog board stick together to form a single board physically. The microwave board contains all the RF components, interconnects, and transitions. RF component includes but not limited to LNA, PA, phase shifter, multifunctional chip, filters, and multiplexer. The analog board, on the other hand, integrates the low-frequency components such as power management IC and signal processing unit, to name a few. With the proposed multilayer PCB technology, it is possible that carefully designed microwave and analog boards can be assembled directly, obviating the need for much shielding between each other which is conventionally added for electromagnetic inference suppression. In the meantime, it helps us to improve installation speed and hardware reliability for mass production.

Figure 4 shows the exploded view of the assembled T/R module. The multilayer board is inserted and fixed to the cavity, and a metal plate is placed on top of it for mechanical protection. Nine SMP connectors and a 21-pin low-frequency socket are designed at the two sides of the module.

In order to improve the stability of the devised system, several treatments are applied. Firstly, a time division DC regulation mechanism is adopted. To be specific, the transmitting and receiving circuitries never operate at the same time. By doing so, mutual interference between the two modes is greatly mitigated. Secondly, comprehensive electromagnetic and simulations are conducted and metallic walls and absorptive materials are added to prevent unwanted cavity resonance. Thirdly, strip lines are widely used to isolate microwave circuits from digital and low-frequency analog circuits. The overall dimension of the fabricated eight-channel T/R module is 83 mm × 24 mm × 9.3 mm. Figure 5 gives the 3D assembly view of the whole structure.

3.2. Thermal Management. Proper thermal design is of crucial importance for space application in which unwanted heat should be dissipated efficiently. For first contribution to this issue, two fans are applied at the air inlet to have a supply air rate of 84 m^3/h and a maximum pressure of 560 Pa. Besides, a series of fins are arranged in each TR air duct to take away the heat. The thickness of fins is thinned to 0.75 mm, while

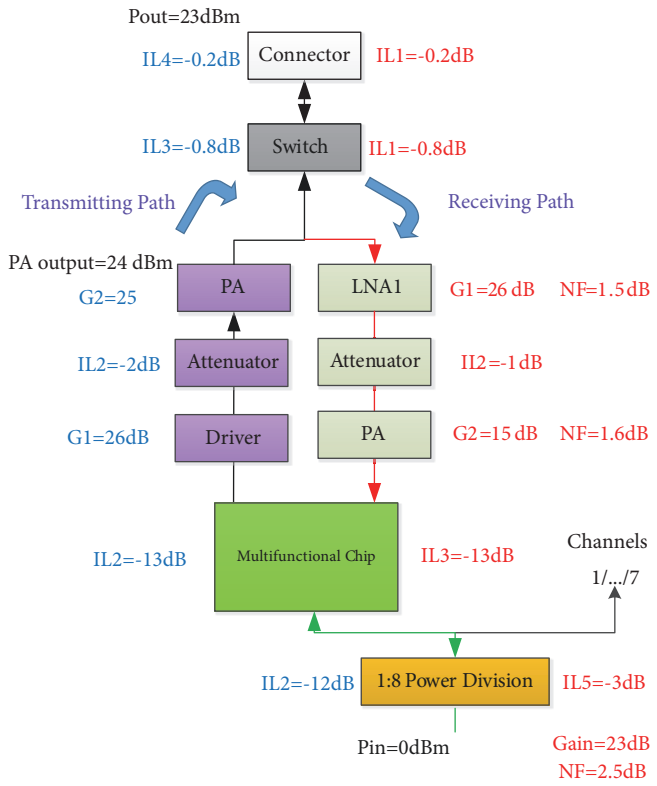

Figure 3: Basic system specification distribution diagram of the proposed AESA.

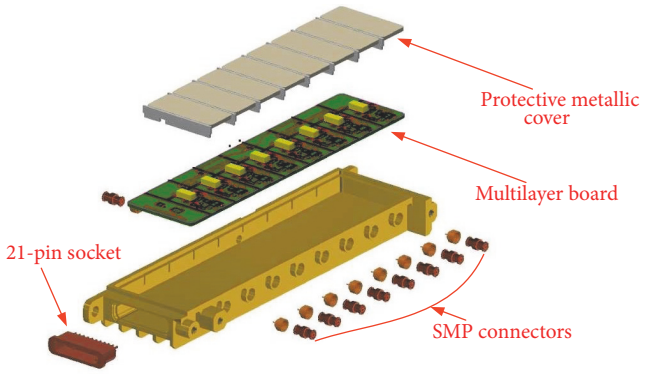

Figure 4: Exploded view of the design of 3D T/R module.

the spacing between adjacent fins is optimized to be 2 mm. These two strategies help us to improve dissipation area. Moreover, the T/R and power modules are soldered directly to the metallic structure using AuSn alloy instead of epoxy resin. For better demonstration, thermal simulations are conducted in ANSYS Workbench to validate the above design considerations. Figure 6(a) shows the simulated temperature distribution of the package. For an ambient temperature of 40°C, the peak chip temperature is around 68°C. Figure 6(b) depicts the transient thermal analysis result. As one can see, the maximum temperature can be achieved and stabilized in roughly 300 seconds after system starts up, fully validating the effectiveness of heat design.

3.3. Ku-Band Antenna Array Design on LTCC. In order to keep the entire active electronically steerable antenna compact, light, and easy to integrate and install, a patch antenna array composed of 8 × 8 radiated elements is constructed on the top of AESA with a microwave LTCC substrate. A microstrip power divider with 90° phase difference outputs as well as the slot coupling technique is used to feed each element for realizing right-handed circular polarization [19]. The proposed antenna array is designed individually and connects with the T/R module via SSMP. The circularly polarized radiator is designed to operate at 15.5 GHz with a bandwidth of more than 1 GHz, which is fed by a probe along the diagonal line of the rectangular patch. The distances along the azimuth and range directions between the elements are 9.5 mm, which is about half of wavelength at 15.5 GHz so as to avoid strong coupling. Each radiator is independently controlled by a suit of T/R module so that the amplitude and the phase of the excitation of each radiator can be tuned continuously.

4. Simulation and Measurement Results

To demonstrate the functionality of the proposed AESA, a prototyping system is manufactured and tested. Figure 7 shows a photograph of the fabricated antenna array. The devised systems are measured in a microwave anechoic chamber. A remote-controlled laptop is connected to it, which conveniently sends the required configuration commands to the systems.

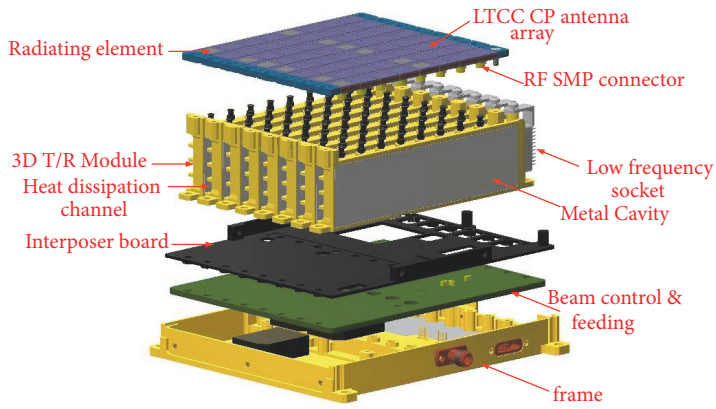

FIGURE 5: 3D assembly view of the whole structure.

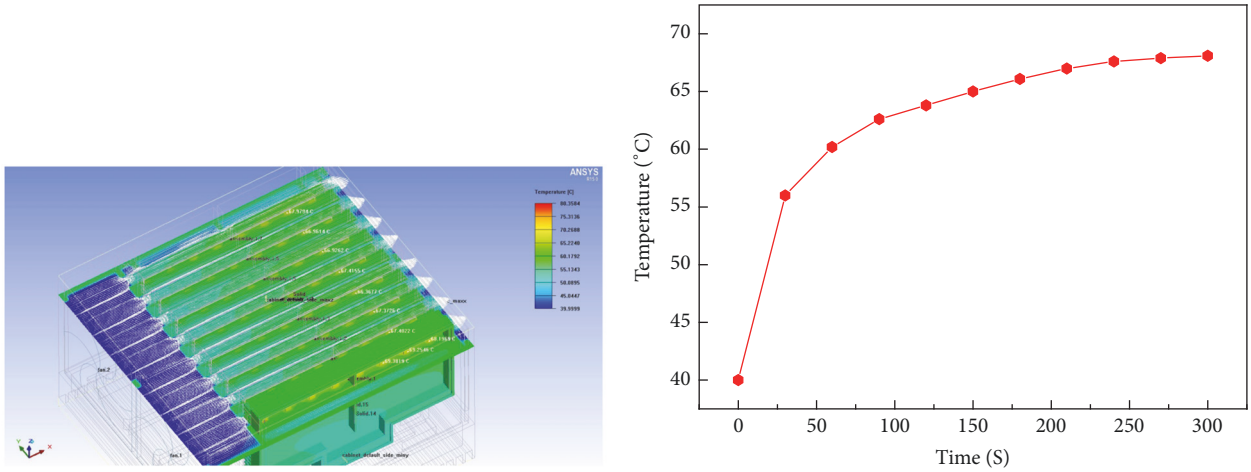

(a) (b)

FIGURE 6: Thermal simulation results: (a) package temperature distribution and (b) transient thermal response.

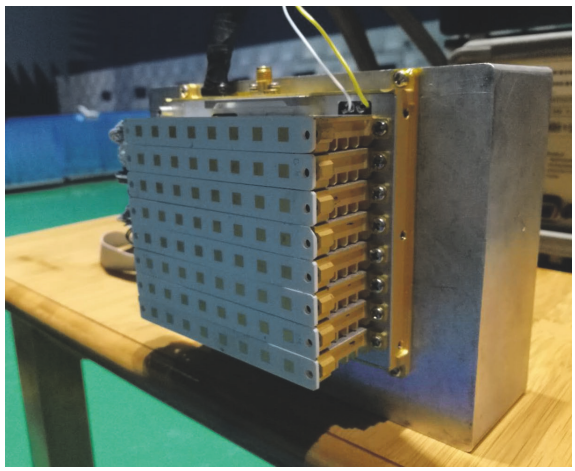

FIGURE 7: Photograph of the implemented ASEA.

The proposed 8 × 8 array antenna is simulated and optimized with HFSS. And the voltage standing wave ratios (VSWRs) of the proposed AESA (excluding the active parts) are measured using Agilent E8363B vector network analyzer.

As indicated in Figure 8, most of the simulated and measured VSWRs are below 1.5 at the operating band (from 15 GHz to 16 GHz) and good agreements are achieved between the two sets of results, where the slight differences are still acceptable and are most likely caused by the discrepancy in the permittivity of the substrate, the unbalanced coaxial cable feeding, and the uncertain factors during manufacturing. These results prove that the proposed AESA exhibits a good electrical performance.

The measured and simulated axial ratios (ARs) are depicted in Figure 9. It is readily seen that the proposed antenna achieves a 0.5 GHz bandwidth with the axial-ratio bandwidth of AR < 3 dB (from 15.25 GHz to 15.75 GHz). There is some discrepancy between the simulated and the measured results owing to some unbalanced phase shifts in the fabricated feeding network. However, the bandwidth of the simulated and measured results tends to be of the same level.

The simulated and measured radiation patterns at the center frequency, i.e., 15.5 GHz, at different steering angles,

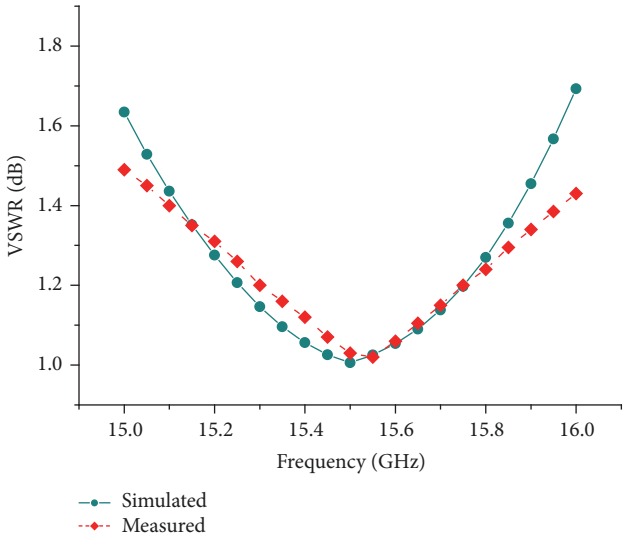

FIGURE 8: Return loss of the proposed ASEA (simulated and measured results).

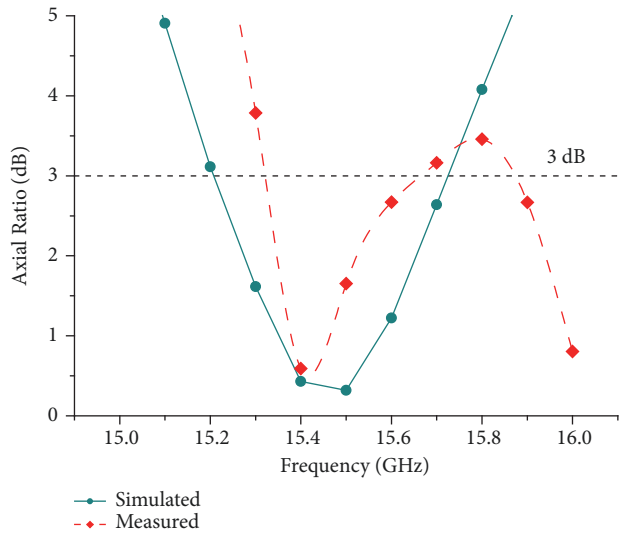

FIGURE 9: Measured axial ratio of the ASEA (simulated and measured results).

are plotted in Figure 10. In these cases, it can be seen that the proposed AESA can steer the pencil beams from -60 degrees to 60 degrees, while keeping the side lobe below about -11 dBc. It is readily observed that the measured radiated patterns are in good agreement with the simulated data. And, at both of transmitting and receiving states, the proposed ASEA keeps almost the same radiation patterns, which ensures the performance of the transceiver systems.

The antenna gain is measured including the factors such as cable loss, feeding network, and reflection loss. Figure 11 shows the simulated and measured gains at the operating frequency band. In the frequency band 15-16 GHz, the measured gain varies from 22 to 24 dBi and the average of gain is about

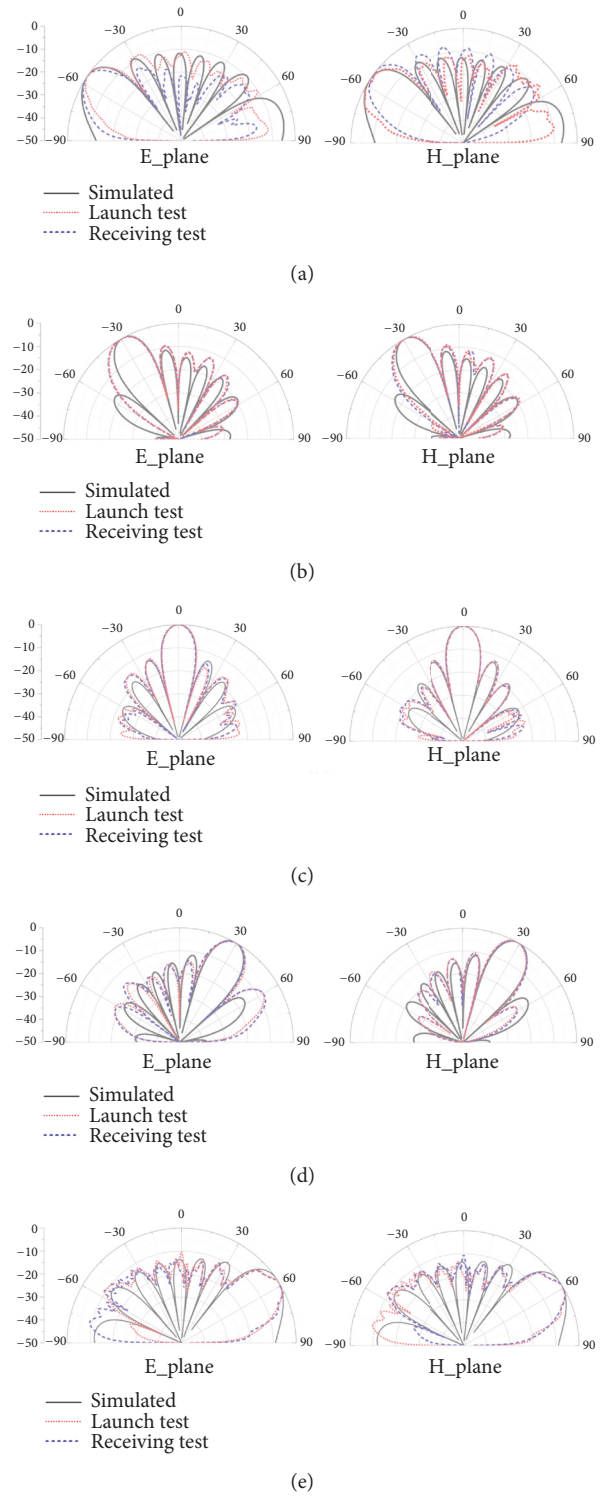

FIGURE 10: Electronically steerable 2D patterns of the proposed ASEA at 15.5 GHz: (a) AZ_-60°; (b) AZ_-30°; (c) AZ_0°; (d) AZ_30°; and (e) AZ_60°.

23 dBi. There is some slight deviation between the simulated and the measured gain, which may be due to the losses of substrate and inaccurate modeling between the simulation and fabrication.

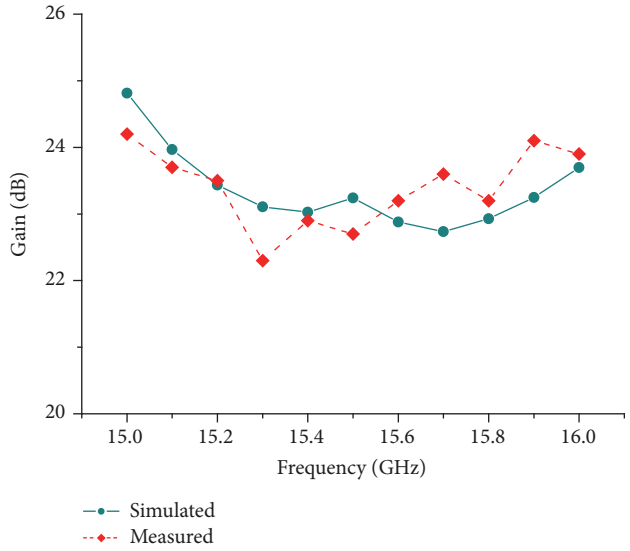

Figure 11: Gain of the proposed ASEA (simulated and measured results).

5. Conclusion

In this work, a Ku-band AESA based on 3D T/R module and LTCC patch antenna array has been introduced. By assembling two boards for different purposes into a whole multilayer board, the 3D T/R technique improved system integration and reduced implementation cost and size. Besides, a wideband circular polarized antenna array was designed in LTCC and connected to the proposed T/R modules to form a complete AESA. Measurement results showed very good phased array performances.

Data Availability

The data used to support the findings of this study are available from the corresponding author upon request.

Conflicts of Interest

The authors declare that they have no conflicts of interest.

Acknowledgments

This work was supported by the National Natural Science Foundation of China under Grant 61601160 and Grant 61601161 and in part by the Zhejiang Provincial Natural Science Foundation of China under Grant LY19F010013.

References

[1] J. Li, Z. He, J. Plaza et al., "Social media: new perspectives to improve remote sensing for emergency response," *Proceedings of the IEEE*, vol. 105, no. 10, pp. 1900–1912, 2017.

[2] M. Martorella, D. Pastina, F. Berizzi, and P. Lombardo, "Spaceborne radar imaging of maritime moving targets with the Cosmo-SkyMed SAR system," *IEEE Journal of Selected Topics in Applied Earth Observations and Remote Sensing*, vol. 7, no. 7, pp. 2797–2810, 2014.

[3] L. Corucci, A. Meta, and A. Coccia, "An X-band radar-based airborne collision avoidance system proof of concept," in *Proceedings of the 2014 15th International Radar Symposium, IRS 2014*, pp. 1-2, Poland, June 2014.

[4] A. Moreira, P. Prats-Iraola, M. Younis, G. Krieger, I. Hajnsek, and K. P. Papathanassiou, "A tutorial on synthetic aperture radar," *IEEE Geoscience and Remote Sensing Magazine*, vol. 1, no. 1, pp. 6–43, 2013.

[5] V. Nguyen, H. Nam, Y. Choe, B. Lee, and J. Park, "An X-band Bi-directional transmit/receive module for a phased array system in 65-nm CMOS," *Sensors*, vol. 18, no. 8, p. 2569, 2018.

[6] M. Kirscht, A. Dallinger, J. Mietzner, B. Bickert, J. Hippler, and R. Zahn, "Recent advances in airborne phased array radar systems," in *Proceedings of the 16th International Radar Symposium (IRS)*, pp. 231–235, 2015.

[7] N. Kundtz, K. Corp, and R. Wash, "Next generation communications for next generation satellites," *IEEE Microwave Magazine*, vol. 57, no. 8, pp. 56–64, 2014.

[8] J. Hunt, J. Gollub, T. Driscoll et al., "Metamaterial microwave holographic imaging system," *Journal of the Optical Society of America A: Optics and Image Science, and Vision*, vol. 31, no. 10, pp. 2109–2119, 2014.

[9] B. Bonnet, P. Monfraix, R. Chiniard et al., "3D packaging technology for integrated antenna front-ends," in *Proceedings of the 2008 European Microwave Integrated Circuit Conference (EuMIC)*, pp. 542–545, Amsterdam, Netherlands, October 2008.

[10] M. Hauhe and J. Wooldridge, "High density packaging of X-band active array modules," *IEEE Transactions on Components, Packaging, and Manufacturing Technology: Part B*, vol. 20, no. 3, pp. 279–291.

[11] S.-K. Yeo, J.-H. Chun, and Y.-S. Kwon, "A 3-D X-band T/R module package with an anodized aluminum multilayer substrate for phased array radar applications," *IEEE Transactions on Advanced Packaging*, vol. 33, no. 4, pp. 883–891, 2010.

[12] A. Di Carlofelice, F. De Paulis, A. Fina, U. Di Marcantonio, A. Orlandi, and P. Tognolatti, "Compact and reliable T/R module prototype for advanced space active electronically steerable antenna in 3-D LTCC technology," *IEEE Transactions on Microwave Theory and Techniques*, vol. 66, no. 6, pp. 2746–2756, 2018.

[13] A. E. I. Lamminen, J. Säily, and A. R. Vimpari, "60-GHz patch antennas and arrays on LTCC with embedded-cavity substrates," *IEEE Transactions on Antennas and Propagation*, vol. 56, no. 9, pp. 2865–2874, 2008.

[14] J. Xu, Z. N. Chen, X. Qing, and W. Hong, "Bandwidth enhancement for a 60 ghz substrate integrated waveguide fed cavity array antenna on LTCC," *IEEE Transactions on Antennas and Propagation*, vol. 59, no. 3, pp. 826–832, 2011.

[15] T. Seki, N. Honma, K. Nishikawa, and K. Tsunekawa, "A 60-GHz multilayer parasitic microstrip array antenna on LTCC substrate for system-on-package," *IEEE Microwave and Wireless Components Letters*, vol. 15, no. 5, pp. 339–341, 2005.

[16] Y. Zhang, M. Sun, K. M. Chua, L. L. Wai, D. Liu, and B. P. Gaucher, "Antenna-in-Package in LTCC for 60-GHz Radio," in *Proceedings of the 2007 International workshop on Antenna Technology: Small and Smart Antennas Metamaterials and Applications*, pp. 279–282, Cambridge, UK, March 2007.

[17] D. G. Kam, D. Liu, A. Natarajan, S. Reynolds, H.-C. Chen, and B. A. Floyd, "LTCC packages with embedded phased-array

antennas for 60 GHz communications," *IEEE Microwave and Wireless Components Letters*, vol. 21, no. 3, pp. 142–144, 2011.

[18] Analysis and design of RF and digital systems using keysight SystemVue, Keysight App Note, https://literature.cdn.keysight.com/litweb/pdf/5992-0197EN.pdf.

[19] R. Caso, A. Buffi, M. Rodriguez Pino, P. Nepa, and G. Manara, "A novel dual-feed slot-coupling feeding technique for circularly polarized patch arrays," *IEEE Antennas and Wireless Propagation Letters*, vol. 9, pp. 183–186, 2010.